

Valence States and Structure of Mixed-Valence Dinuclear Iron(II,III) Complexes $[Fe_2(2,6\text{-bis[bis(2-pyridylmethyl)aminomethyl]-4-methylphenol})(L)_2](BF_4)_2$

Yonezo Maeda,* Akiko Ishida, Masaaki Ohba, Shinji Sugihara, and Shinya Hayami

Department of Chemistry, Faculty of Sciences, Kyushu University, Hakozaki, Higashi-ku, Fukuoka 812-8581

(Received May 13, 2002)

Mixed-valence dinuclear iron(II,III) complexes, $[Fe^{II}Fe^{III}(bpmp)(L)_2](BF_4)_2$, have been prepared, and the structures, electrochemical properties and rates of intramolecular electron transfer of the complexes have been examined, where Hbpmp represents 2,6-bis[bis(2-pyridylmethyl)aminomethyl]-4-methylphenol and L is 2-methoxybenzoate (**omb**), 3-methoxybenzoate (**mmb**), 4-methoxybenzoate (**pmb**), 3,5-dimethoxybenzoate (**dmb**), 3,4,5-trimethoxybenzoate (**tmb**) or 4-biphenylcarboxylate (**bpc**). It turns out from the Mössbauer spectra that the valence states of iron atoms of $[Fe^{II}Fe^{III}(bpmp)(omb)_2](BF_4)_2$, $[Fe^{II}Fe^{III}(bpmp)(pmb)_2](BF_4)_2$, $[Fe^{II}Fe^{III}(bpmp)(tmb)_2](BF_4)_2$ and $[Fe^{II}Fe^{III}(bpmp)(bpc)_2](ClO_4)_2$ are localized at 78 K and delocalized at 293 K. The temperature dependence of the spectra is interpreted by assuming intramolecular electron transfer between two energetically equivalent vibronic states $Fe_A^{II}Fe_B^{III}$ and $Fe_A^{III}Fe_B^{II}$. The Mössbauer spectra of $[Fe^{II}Fe^{III}(bpmp)(dmb)_2](BF_4)_2$ show the superposition of the relaxation spectrum between iron(II) and iron(III), and of the spectrum of the average valence states at 293 K; the average valence states are partly observed even at 78 K. The valence states of $[Fe^{II}Fe^{III}(bpmp)(mmb)_2](BF_4)_2$ are localized over the temperature range from 78 K to 293 K. The single-crystal X-ray structure of $[Fe^{II}Fe^{III}(bpmp)(bpc)_2](ClO_4)_2$ was determined at 293 K. The complex crystallizes in the orthorhombic space group Fdd2, which has a unit cell of $a = 27.056(1)$ Å, $b = 42.652(0)$ Å, $c = 12.151(0)$ Å and $Z = 8$. A refinement was performed with 2340 unique reflections [$I > 3\sigma(I)$] to give $R = 0.085$, $R_w = 0.099$. The two iron atoms are located symmetrically to a C_2 axis, which presents in the molecule, and are crystallographically equivalent. The mean Fe–O length is intermediate between the Fe^{II}–O and Fe^{III}–O values, indicating that both iron atoms are in an averaged valence state.

Carboxylate-bridged binuclear iron complexes with a variety of multidentate ligands have been intensively studied, since it is known that dinuclear iron clusters in the active sites of metalloproteins play an important role, such as reversible dioxygen binding or activation. Significant examples are haemerythrin (Hr),[1,2] the R2 subunit of ribonucleotide reductase (RNR),[3] the hydroxylase component (H) of methane monooxygenase (MMO),[4–6] and purple acid phosphatase (PAPs).[7,8] In order to comprehend the structural and spectroscopic properties of those diiron centers, mixed-valence binuclear iron(II,III) complexes with a heptadentate polypyridine ligand (Hbpmp) were synthesized by Suzuki et al.,[9,10] and diiron(II,III) complexes which contain imidazole derivatives instead of the pyridine groups (Hbimp),[11] or which contain two phenol groups substituted for two pyridine groups (Hbbpmp),[12] have been also reported.

The goal of the investigations of the "bpmp" complexes is to elucidate not only the valence states in solid state, but also the properties of model compounds for biological systems, because carboxylic acid is contained in a living thing and complexes with carboxylic acids having a long chain ($Ph(CH_2)_nCOOH$, $n \geq 3$) show delocalized valence states above 260 K.[13] It is all the more significant for an understanding of the electron-transfer events in biological systems to know the mechanism of the temperature dependence of the electron transfer rate between two iron atoms of $Fe^{II}Fe^{III}$ bpmp complexes.

It has been reported that the motion of amino acid moieties at a rate of 10^2–10^4 s^{-1} in a region near to heme modulates the rate of electron transfer,[14] and that fast photoinduced intramolecular electron transfer occurs at a center-to-center separation of up to 13.3 Å in a series of rigid non-conjugated bridges.[15] In addition to the discussion about how fast the reorganization of moieties occurs in cations, anions and/or solvents associated with electron transfer in mixed-valence complexes occurs is of interest. Mössbauer spectra collected for $Fe^{II}Fe^{III}$ bimp complexes clearly show the sensitivity of these complexes to anions, bridging ligands and solvents, and those for Fe_2bpmp complexes show sensitivity to bridging ligands. The rates of electron transfer in a solid are sensitive to the packing environment because the coupling of the electronic and vibrational coordinates leads to sensitivity to the environment. Kambara and Sasaki have reported that the interaction between the molecular distortions in different molecules is essential to the transitions.[16] Adachi et al. have proposed the effect of an unusual type of quenched disorder on phase transitions for $Fe^{II}{}_2Fe^{III}O$ complexes.[17a] It should be noted that the packing environment, including the rearrangement of iron moieties of mixed-valence complexes, is an important factor for determining the rate of intramolecular electron transfer.

Hendrickson et al.[18] and Sano et al.[19] have systematically investigated the structures and valence states of mixed-valence

bis(ferrocene) derivatives and trinuclear iron carboxylates by means of the ^{57}Fe Mössbauer technique, X-ray diffraction analysis, heat capacity measurement and so on. They have made it clear that the rates of electron transfer are sensitively influenced by the crystal packing. Most of the complexes give valence-delocalized spectra accompanied by line broadening due to a gradual increase in the electron-exchange rates, as observed in $Fe^{II}Fe^{III}$ bpmp and bimp complexes. On the other hand, "fusion type" Mössbauer spectra, where two quadrupole doublets move together to become a single averaged doublet without any significant line broadening, were observed in some biferrocene derivatives and trinuclear iron carboxylates.[18,19] Furthermore, in bis(ferrocenium)dibromoiodate, a third averaged doublets appears in addition to Fe^{II} and Fe^{III} doublets and grows with increasing temperature until ~340 K, at which point only an averaged doublet is seen.

These mixed-valence complexes consist of high-spin iron(II) and high-spin iron(III) at 78 K, except for complex **4**, and the mixed-valence states are observed at 293 K, except for complex **2**. Furthermore, dinuclear iron complexes composed of low-spin iron(II) and low-spin iron(III) have been reported by Spreer et al.[20] and an intense near-infrared band due to an intervalence transition (IT band) is observed. In contrast, diiron complexes with a nonadentate polypyridine ligand, which has stronger ligand field than bpmp, were synthesized by our group,[13d] and indicated no observable band due to an intervalence transition between a high-spin iron(II) and a low-spin iron(III). $[Fe(bpmp)(PhCOO)_2](BF_4)_2$ shows localized valence states at 293 K[13e] and $[Fe(bpmp)(4\text{-}CH_3OPhCOO)_2](BF_4)_2$ shows delocalized valence states at 293 K; the structure has been determined.[13e] In order to clarify the mechanism of the electron-transfer rate, complexes with a similar chemical structure to that shown in Fig. 1 were prepared, and the electron-transfer rate was examined from the Mössbauer spectra.

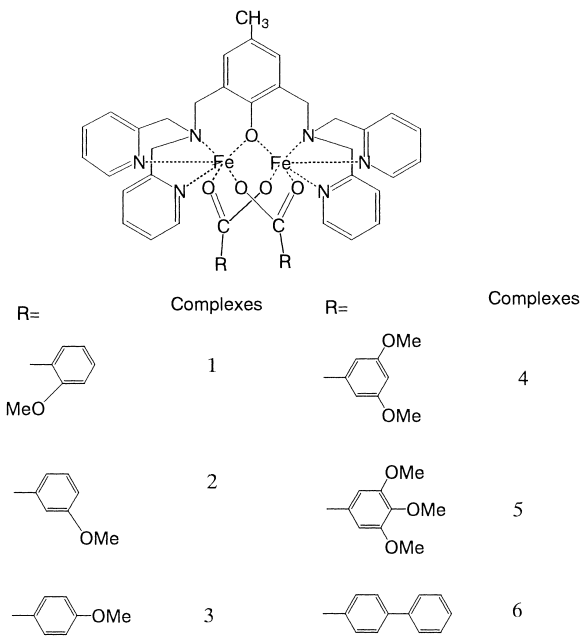

Fig. 1. Chemical structures of $[Fe_2(bpmp)(RCOO)_2]^{2+}$ and carboxylic acids.

Experimental

Synthesis. The preparation of 2,6-bis[bis-(2-pyridylmethyl)-aminomethyl]-4-methylphenol (Hbpmp) is described elsewhere.[13c] Those complexes isolated as perchlorate salts should be handled as potentially explosive compounds.

$[Fe^{II}Fe^{III}(bpmp)(bpc)_2](ClO_4)_2$, 6. Synthesis of **6** is described in detail as a representative. The complexes were prepared using a deoxygenated methanol solution under a nitrogen atmosphere. A methanol (30 mL) solution of iron(II)perchlorate hexahydrate (726 mg, 2 mmol) was added to a methanol (30 mL) solution of Hbpmp (530 mg, 1 mmol) with stirring, and then 4-biphenylcarboxylic acid (396 mg, 2 mmol) and triethylamine (151 mg, 1.5 mmol) were added. The solution was exposed to an oxygen atmosphere with stirring. Dark-green precipitates were collected by filtration, washed with ethanol and ether, and dried in a vacuum. The complexes were obtained as dark-green precipitates. Found: C, 57.92; H, 4.23; N, 7.01; Fe, 9.35%. Calcd for $C_{59}H_{53}N_6O_{13}Cl_2Fe_2$. C, 57.30; H, 4.29; N, 6.80; Fe, 9.04%. μ_{eff} per 2Fe: 7.83 μ_B at 290 K. Selected IR (ν_{max}/cm^{-1}): 1606 (ν(C=N)), 1576 (ν_{asymm}(C=O)), 1364, 1395 (ν_{symm}(C=O)), Molar conductance (Λ_M/S cm^2 mol^{-1}): 322 in acetonitrile.

$[Fe^{II}Fe^{III}(bpmp)(omb)_2](BF_4)_2\cdot 2H_2O$, **1**. Found: C, 51.03; H, 4.31; N, 7.25; Fe, 9.50%. Calcd for $C_{49}H_{51}N_6O_9B_2F_8Fe_2$: C, 51.03; H, 4.46; N, 7.29; Fe, 9.69%. $[Fe^{II}Fe^{III}(bpmp)(3\text{-}mmb)_2](BF_4)_2$, **2**. Found: C, 52.18; H, 4.25; N, 7.44; Fe, 9.94%. Calcd for $C_{49}H_{47}N_6O_7B_2F_8Fe_2$: C, 52.68; H, 4.24; N, 7.52; Fe, 10.00 %. $[Fe^{II}Fe^{III}(bpmp)(pmb)_2](BF_4)_2$, **3**. Found: C, 53.00; H, 4.22; N, 7.21; Fe, 9.50%. Calcd for $C_{49}H_{47}N_6O_7B_2F_8Fe_2$: C, 52.67; H, 4.21; N, 7.52; Fe, 10.00%. $[Fe^{II}Fe^{III}(bpmp)(dmb)_2](BF_4)_2$, **4**. Found: C, 52.66; H, 4.34; N, 7.73; Fe, 10.02%. Calcd for $C_{51}H_{51}N_6O_9B_2F_8Fe_2$: C, 52.02; H, 4.33; N, 7.14; Fe, 9.50%. $[Fe^{II}Fe^{III}(bpmp)(tmb)_2](BF_4)_2$, **5**. Found: C, 51.56; H, 4.56; N, 6.36; Fe, 9.13%. Calcd for $C_{53}H_{55}N_6O_{11}B_2F_8Fe_2$: C, 51.44; H, 4.45; N, 6.79; Fe, 9.04%.

Physical Measurements. Microanalyses for carbon, hydrogen, and nitrogen were carried out at the Elemental Analysis Center, Kyushu University. A quantitative analysis for iron was performed by an atomic-absorption analysis, using an Atomic Absorption/Flame Emission Spectrometer AA-625-11 (Shimadzu).

The magnetic susceptibility on polycrystalline samples was measured by the Faraday method, using an electrovalence type 2002 (Cahn Instrument) with an electromagnet (8,000G) operated at 20 A. The temperature was controlled at over 80–300 K using a digital temperature controller model 3700 (Scientific Instruments). $HgCo(NCS)_4$ was used as a calibration substance. The effective magnetic moment was calculated by the formula $\mu_{eff} = 2.83\ (\chi_M T)^{1/2}$, where χ_M is the molar susceptibility after applying diamagnetic corrections.

Mössbauer spectra were measured with an S-600 constant-acceleration spectrometer (Austin Science Associates). The temperature was controlled with a temperature controller (ITC502, Oxford Instruments) within a variable temperature cryostat (DN1726, Oxford Instruments). The data were stored in a 1024-channel analyzer (IT-5200, Inotech Inc.). A 10 mCi cobalt-57 source diffused into a palladium foil was used. The spectra were fitted by a Lorentzian line shape using software of IGOR Pro (WaveMetrics, Inc) on a personal computer. The least-squares fitting for spectra with two or three pairs of doublets was calculated under the constraint that the doublets have equal intensities and equal full widths at half maximum of each other, except for the simulation for complex **3**. The velocity scales and isomer shifts

were normalized to iron foil at room temperature.

Absorption and reflection spectra were measured in the region from 400 to 2000 nm using a Shimadzu UV-3100PC self-recording spectrophotometer.

Cyclic voltammetry of the complexes in acetonitrile was carried out on an AC/DC Cyclic Polarograph P-900 (Yanaco) at 293 K under an argon atmosphere. A standard three-electrode system (BAS) was employed comprising a glassy carbon working electrode, an Ag-Ag^+–MeCN–NBu_4ClO_4 (RE-5, BAS) reference electrode and a platinum counter electrode. Ferrocene was used as a standard substance. The observed values were converted to redox potentials versus SCE by using the following equation:

Redox potential for the complexes
= observed value for a complex − observed value for ferrocene
+ 0.0739 (ferrocene vs Ag/Ag^+) + 0.272 (SCE vs Ag/Ag^+) (1)

Single-Crystal X-ray Structure Analysis. An x-ray structure determination of **6** was carried out at 293 K. A dark-green single crystal (0.65 × 0.30 × 0.25 mm) of **6** was mounted on a Rigaku 7S four circle diffractometer equipped with a liquid-N_2 cryostream cooler (Oxford Cryosystems). Graphite monochromatized Mo-$K\alpha$ radiation ($\lambda = 0.71069$ Å) was used for the measurement. All data were corrected for Lorentz and polarization effects, and empirical absorption corrections (ω–2θ scans) were carried out in each case. The numbers of measured reflections were 4225, with 2340 unique reflections [$I > 3\sigma(I)$]. No decay in the intensity was observed during the measurements. The lattice constants were optimized from a least-squares refinement of the settings of 25 carefully centered Bragg reflections in the range of $25° < 2\theta < 30°$. Crystallographic data are given in Table 1. The structures were solved by the direct method and Fourier techniques, and refined by a full-matrix least-squares method. All non-hydrogen atoms were readily located and refined with anisotropic thermal parameters. An ORTEP drawing of the cation with its atom-labeling scheme is given in Fig. 2. Hydrogen atoms were located from structure-factor calculations. A C_2-axis is present in the C(1)–C(2)–C(5)–O(1) axis, and the calculated hydrogen atoms of C(1) atom are not just on the axis. Therefore, three hydrogen atoms, the populations of which are 0.5, are deposited on the C(1) atom before applying a symmetry expansion. The final refinements gave $R = 0.085$, $R_w = 0.099$. The CIF data for the crystal are deposited as Document No.75051 at the Office of the Editor of Bull. Chem. Soc. Jpn. Crystallographic data have been deposited at the CCDC, 12 Union Road, Cambridge CB2 1EZ, UK and copies can be obtained on request, free of charge, by quoting the publication citation and the deposition number 165088.

Results and Discussion

Single-Crystal X-ray Structure of 6. A single-crystal structure determination of **6** was carried out at 293 K. The atomic parameters (Table I), anisotropic thermalparameters (Table II), and selected bondlengths and angles (Table III) are kept as supplemental materials in the editorial office. The iron atoms in the cation are bridged with an oxygen atom of phenolate and oxygen atoms of two carboxylates, and located in a distorted N_3O_3 octahedron. A C_2-axis is present in C(1)–C(2)–C(5)–O(1) of the molecule. The two iron atoms are crystallographically equivalent. The selected bond distances and angles are listed in Table 2. The Fe···Fe distance is 3.372(3) Å, being similar to 3.365(7) Å of $[Fe^{II}Fe^{III}(bpmp)\{CH_3(CH_2)_5CO_2\}_2]$-

Table 1. Crystal Data and Structure Refinement Details for Complex **6**

Empirical formula	$C_{67}H_{61}N_{10}O_{13}Fe_2Cl_2$
Formula weight	1396.88
Crystal color, habit	Green, prismatic
Crystal dimensions	0.65 × 0.30 × 0.25 mm
Temperature	293 K
Crystal system	Orthorhombic
Lattice type	*F*-centered
Lattice parameters	$a = 27.056(1)$ Å
	$b = 42.652(0)$ Å
	$c = 12.151(0)$ Å
	$V = 14027(2)$ Å^3
Space group	Fdd2 (#43)
Z value	8
D_{calc} / g cm^{-3}	1.323 g cm^{-3}
D_{obs} / g cm^{-3}	1.353 g cm^{-3}
μ (Mo $K\alpha$)	5.56 cm^{-1}
Diffractometer	Rigaku AFC7R
Radiation	Mo $K\alpha$ ($\lambda = 0.71069$ Å)
	graphite monochromated
Scan type	ω–2θ
No. of reflection measured	Total: 4225
	Unique: 2340
Structure solution	Direct methods
p-factor	0.025
No. observations ($I > 3.00\sigma(I)$)	2361
No. variables	346
Residuals: $R^{a)}$; $R_w{}^{b)}$	0.085; 0.099
Goodness of fit indicator	4.00
Max shift / error in final cycle	0.17

a) $R = \Sigma||F_o|-|F_c||/\Sigma|F_o|$. b) $R_w = [\Sigma w(F_o{}^2-F_c{}^2)^2/\Sigma w(F_o{}^2)^2]^{1/2}$.

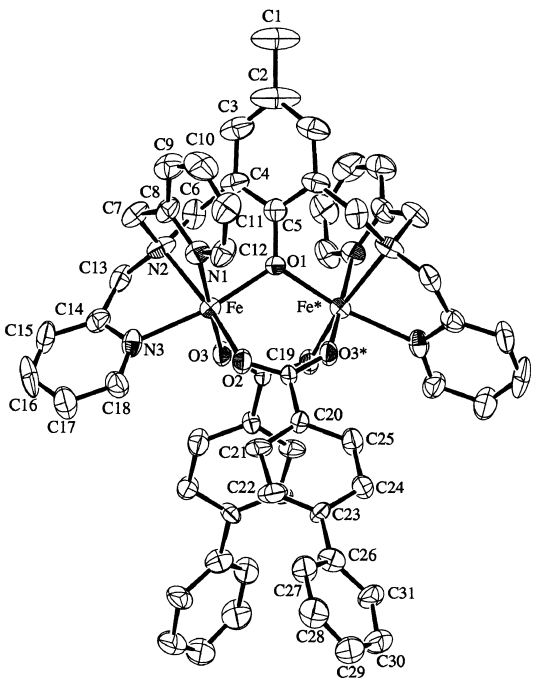

Fig. 2. Ortep drawing of complex **6**.

Table 2. Selected Bond Lengths and Angles for Complex **6**

	Bond lengths (Å)		
Fe–O(1)	1.997(6)	Fe–O(2)	1.981(8)
Fe–O(3)	2.060(8)	Fe–N(1)	2.177(9)
Fe–N(2)	2.201(9)	Fe–N(3)	2.167(9)
	Bond angles (°)		
O(1)–Fe–O(2)	100.2(3)	O(1)–Fe–O(3)	90.3(3)
O(1)–Fe–N(1)	86.8(3)	O(1)–Fe–N(2)	89.2(3)
O(1)–Fe–N(3)	163.9(3)	O(2)–Fe–O(3)	93.7(3)
O(2)–Fe–N(1)	91.8(3)	O(2)–Fe–N(2)	166.7(3)
O(2)–Fe–N(3)	95.0(3)	O(3)–Fe–N(1)	174.1(4)
O(3)–Fe–N(2)	95.7(3)	O(3)–Fe–N(3)	83.5(3)
N(1)–Fe–N(2)	79.2(4)	N(1)–Fe–N(3)	97.9(3)
N(2)–Fe–N(3)	76.8(4)	Fe–O(1)–Fe	115.1(5)

$(BF_4)_2$[13e] and 3.365(1) Å of $[Fe^{II}Fe^{III}(bpmp)(CH_3CH_2CO_2)_2](BPh_4)_2$.[11d] The average Fe–O(1) value is 1.997(6), being intermediate between the Fe^{II}–O and Fe^{III}–O bond lengths. Therefore, it can be said that the two iron atoms are in an averaged valence state at 293 K. The Fe–O(2) and Fe–O(3) are 2.060(8) Å and 1.981(8) Å, respectively. The average Fe–O distance is shorter than the corresponding ones of other Fe_2bpmp complexes. Fe–N_{amine} bond length (Fe–N(2) = 2.201(9) Å) is close to 2.233(7) Å of $[Fe^{II}Fe^{III}(bpmp)\{CH_3(CH_2)_5CO_2\}_2](BF_4)_2$[13c] and 2.190(3) and 2.195(3) Å of $[Fe^{II}Fe^{III}(bpmp)\{Ph(CH_2)_3CO_2\}_2](BF_4)_2$,[13e] and 2.195(3) and 2.185(3) Å of $[Fe^{II}Fe^{III}(bpmp)(CH_3CH_2CO_2)_2](BPh_4)_2$.[11d] Average Fe–$N_{pyridine}$ bond length (Fe–N(1), and Fe–N(3)) 2.172(9) Å is longer than 2.158(3) Å of $[Fe^{II}Fe^{III}(bpmp)\{Ph(CH_2)_3CO_2\}_2](BF_4)_2$, 2.166(9) Å of $[Fe^{II}Fe^{III}(bpmp)\{CH_3(CH_2)_5CO_2\}_2](BF_4)_2$ and 2.153(3) Å of $[Fe^{II}Fe^{III}(bpmp)(CH_3CH_2CO_2)_2](BPh_4)_2$. The Fe–O(1)–Fe angle 115.1(5)° is similar to 115.2(1)° of $[Fe^{II}Fe^{III}(bimp)(PhCO_2)_2](BPh_4)_2\cdot 1.5CH_3CN$,[11a] and is larger than 112.3(4)° of $[Fe^{II}Fe^{III}(bpmp)\{CH_3(CH_2)_5CO_2\}_2](BF_4)_2$ and 113.1(1)° of $[Fe^{II}Fe^{III}(bpmp)(CH_3CH_2CO_2)_2](BPh_4)_2$,[11d] It is usually observed for the Fe_2bpmp and Fe_2bimp complexes that the bond angles of the $N_{pyridine}$–Fe–$N_{pyridine}$ are smaller than that of N_{amine}–Fe–$N_{pyridine}$.

A static geometrical space or dynamic space formed by the movement of more mobile molecules i.e. anions and/or solvents would be necessary for rapid electron transfer between Fe(II) and Fe(III) in a solid. One of two butyric acid molecules of $[Fe^{II}Fe^{III}(bpmp)\{Ph(CH_2)_3CO_2\}_2](BF_4)_2$ is located in another geometrically different pocket formed by the crystal packing. Therefore, the potential energy for electron transfer between $Fe_A^{II}Fe_B^{III}$ and $Fe_A^{III}Fe_B^{II}$ becomes inequivalent. It has been pointed out that the onset of motions of the solvate molecules, ligands, or counter ions is probably influenced by the rate of intramolecular electron transfer in a solid. Another important factor which controls the rate of electron transfer is whether the structure of a mixed-valence cation is symmetric relative to the two iron atoms or is asymmetric. If there is a symmetry axis in the middle of the two iron atoms, such as **3** and **6**, the potential-energy surface for the ground state is symmetrized, and the energies of the two vibronic states, $Fe_A^{II}Fe_B^{III}$ and $Fe_A^{III}Fe_B^{II}$, are identical. The potential-energy barrier to interconvert between the two states becomes small, and the rate of the intramolecular electron transfer gradually becomes faster with an increase in temperature.

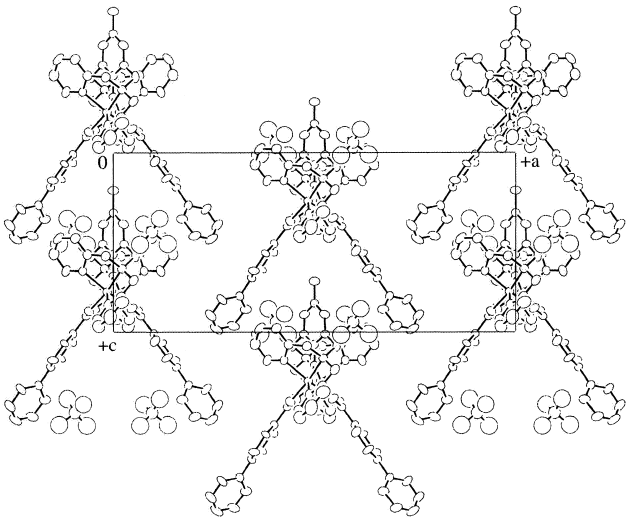

Fig. 3. A packing diagram in the ca plane of complex **6**.

A packing diagram in the ca-plane of **6** is shown in Fig. 3 and the molecules are arranged along to the c-axis, which is also the C_2 axis. The anions are located symmetrically with respect to the C_2 axis. Therefore, the shape of the space around a carboxyl group in the solid is the same as that of the other carboxyl group. In the case of $[Fe^{II}Fe^{III}(bpmp)\{Ph(CH_2)_3CO_2\}_2](BF_4)_2$, the two carboxylic acids coordinating to the cation are inserted in the spaces formed by the arrangement of the neighboring molecules, and the spaces around the two carboxylic acids are entirely different in shape, which makes it difficult to rearrange the iron moieties for electron transfer. The relationship between the crystal structures and mixed-valence states has been studied in bifferocene derivatives: 1′,1″-dibutylbiferrocenium triiodide crystallized in two different forms, one of which shows a conversion from valence trapped to detrapped in the Mössbauer spectra; the other shows trapped spectra at a temperature from 78 K to room temperature. Two crystallographically distinct iron moieties are observed in two forms, and the structure of complexes showing delocalized valence states is more symmetric than that showing localized valence states.

Magnetic Susceptibility. The magnetic susceptibilities of the complexes were measured over the temperature range from 80 to 280 K. The results were analyzed by the usual spin–spin interaction model based on the exchange Hamiltonian, $H = -2J\cdot\mathbf{S}_1\cdot\mathbf{S}_2$. The molar susceptibility (χ_A) of $\mathbf{S}_1 = 2 - \mathbf{S}_2 = 5/2$ spin exchange coupling for dinuclear complexes is given by the following equation:

$$\chi_A = \frac{N\beta^2 g^2}{4\kappa T} \times \frac{x^{24} + 10x^{21} + 35x^{16} + 84x^9 + 165}{x^{24} + 2x^{21} + 3x^{16} + 4x^9 + 5} + N\alpha,$$

where $x = \exp(-J / \kappa T)$ and the symbols have their usual meanings. The J and g values obtained from the temperature dependence of the magnetic susceptibility for **4** are $J = -2.64$ cm^{-1} and $g = 2.14$, and those for **6** J are -1.98 cm^{-1} and $g = 2.56$, suggesting that the iron(II) and iron(III) ions are antifer-

Table 3. Intervalence Transition Bands of the Complexes in Acetonitrile (1×10^{-3} M)

Complexes	λ_{max}	ε_{max}	$\nu_{max}(\times 10)$	$\Delta\nu_{1/2}(\times 10)$	α^2 (10^{-3} mol^{-1})[a)]
1	1324	356	755	468	7.1
2	1306	333	766	425	6.9
3	1408	319	710	417	7.0
4	1358	480	736	440	9.1
5	1312	402	762	432	8.5
6	1272	422	786	485	9.7

a) $\alpha^2 = \dfrac{4.24 \times 10^{-4}\varepsilon_{max}\Delta\nu_{1/2}}{\nu_{max}d^2}$ (d = 3.37 Å).

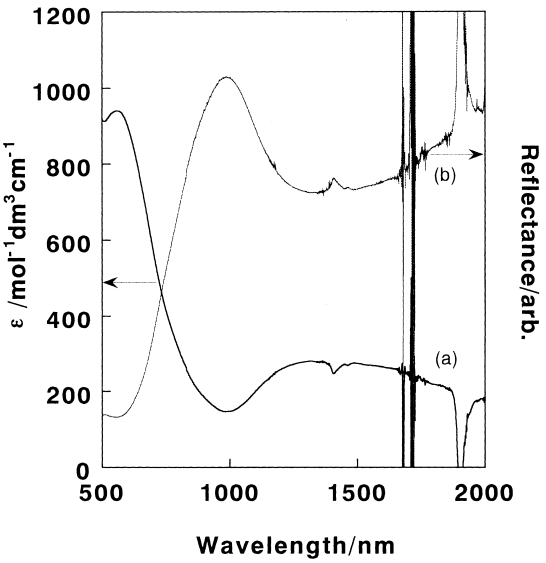

Fig. 4. Absorption and reflectance spectra of complex **1**.

romagnetically coupled to yield an **S** = 1/2 ground state, and that the magnetic interaction between the two iron atoms is very weak.

Reflection and Absorption Spectra. The absorption spectra of **1**–**6** in acetonitrile (ca.1×10^{-3} M) were measured to examine the presence of IT, and the representative spectrum is shown in Fig. 4. Data obtained from the absorption spectra are given in Table 3. The complexes give a band in the visible region (λ = 500–650 nm), which is characteristic of Fe(III)-phenolate complexes. It is assigned to charge-transfer transitions from pπ orbitals of bridging phenolate groups to half-filled dπ* orbitals of Fe(III) ions. The IT bands are observed at around 1300 nm in the absorption spectra. The reflection spectrum of the complexes is similar to the corresponding absorption spectrum, suggesting that the coordinating structure of the iron atom moieties in a solid is maintained in solution.

According to Hush,[21] the delocalization coefficient, (α^2), a measure of the mixing of oxidation states, can be calculated using

$$\alpha^2 = \frac{4.24 \times 10^{-4}\varepsilon_{max}\Delta\nu_{1/2}}{\nu_{max}d^2} \quad (d = 3.37\ \text{Å})$$

The calculated α^2 values are listed in Table 3, in which the metal–metal distance (d) is estimated from the structure of **6**. These values imply that the delocalization of electrons between Fe(II)–Fe(III) moieties is relatively small, and that the complexes belong to the so-called class III ($\alpha^2 = 10^{-2} - 10^{-6}$) mixed-valence systems.[22]

Table 4. Cyclic Voltammetric Data for the Complexes in Acetonitrile (1×10^{-3} M)

Complexes	$E1$[a)]	$E2$[b)]	$E2 - E1$	K_c[c)]
	V vs SCE		V	
1	−0.187	+0.508	0.695	7.2×10^{11}
2	−0.163	+0.526	0.689	4.5×10^{11}
3	−0.059	+0.618	0.677	2.8×10^{11}
4	−0.149	+0.538	0.687	4.2×10^{11}
5	−0.148	+0.533	0.681	3.3×10^{11}
6	−0.157	+0.523	0.680	3.2×10^{11}

a) For the $Fe^{II}Fe^{II}/Fe^{II}Fe^{III}$ redox couple.
b) For the $Fe^{II}Fe^{III}/Fe^{III}Fe^{III}$ redox couple.
c) Comproportionation constant at 20 °C.

Cyclic Voltammetry. The cyclic voltammograms of the complexes in acetonitrile were measured at 293 K and show two quasi-reversible waves corresponding to $Fe^{II}Fe^{II}/Fe^{II}Fe^{III}$, $E1$ and $Fe^{II}Fe^{III}/Fe^{III}Fe^{III}$, $E2$ couples. Their cyclic voltammetric data are collected in Table 4. Constant-potential coulometry shows that these two redox couples correspond to one - electron redox reactions attributable to Fe^{II}–Fe^{II}/Fe^{II}–Fe^{III} and Fe^{II}–Fe^{III}/Fe^{III}–Fe^{III}. The redox potentials of the complexes are dependent on the species of carboxylic acids. The longer is the alkyl chains of carboxylic acid in $[Fe^{II}Fe^{III}(bpmp)\{Ph(CH_2)_n\text{-}CO_2\}_2](BF_4)_2$, the more negative are the $E1$ and $E2$ values.[13e] The peak-to-peak separations between these two waves are 670–690 mV and the ratios of the oxidation currents (i_{pa}) for the forward scan to the reduction currents (i_{pc}) for the reverse scan are close to unity for both couples. Both values of $E1$ and $E2$ are more negative than those of $[Fe_2(bpmp)\{Ph(CH_2)_n\text{-}CO_2\}_2](BF_4)_2$, and the values of $E2$–$E1$ show that the electron-donating properties of OCH_3 on a phenyl ring bring about instabilities of the mixed-valence states, because those of $[Fe_2(bpmp)\{Ph(CH_2)_nCO_2\}_2](BF_4)_2$ are 700–720 mV.[13e] From the separation of the redox potentials of $E1$ and $E2$, the comproportionation constants (K at 20 °C) of the following reaction were calculated:

$$(Fe^{II}\text{–}Fe^{II}) + (Fe^{III}\text{–}Fe^{III}) \rightleftarrows 2\,(Fe^{II}\text{–}Fe^{III}),$$
$$E2 - E1 = RT/F\cdot\ln K.$$

The values are about an order of $K = 10^{11}$, supporting that the

present mixed-valence complexes are highly stabilized.

Mössbauer Spectra. The temperature dependence of the Mössbauer spectra for the complexes was measured. The Mössbauer spectrum of **1** in Fig. 5 shows the localized valence states of iron(II) (δ =1.15 mm/s, ΔE = 2.43 mm/s) and iron(III) (δ = 0.41 mm/s, ΔE = 0.39 mm/s) at 78 K. The spectrum turns to an asymmetric doublet at 293 K, of which the isomer shift is 0.67 mm/s, assigned to delocalized valence states. The Mössbauer spectrum of **2** is shown in Fig. 6. Iron atoms are in the localized valence states of iron(II) and iron(III) in the temperature range from 78 K to 293 K, respectively. The full widths at half maximum (FWHM) of the spectrum at 293 K are 0.49 mm/s and 0.42 mm/s, being sharper than those (0.64 mm/s, 0.67 mm/s) at 78 K. The broadening at 78 K may have resulted from the disorder of the iron sites and/or a saturation effect. The temperature dependence of **3** is shown in Fig. 7, suggesting that the valences of both iron atoms are delocalized at 293 K. Among these three complexes, complex **3** shows the most rapid rate of intramolecular electron transfer at 293 K. The difference in the chemical structure among the

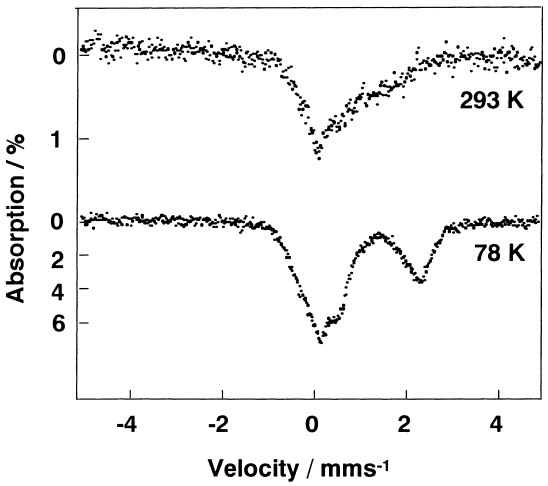

Fig. 5. Temperature dependence of the Mössbauer spectra of complex **1**.

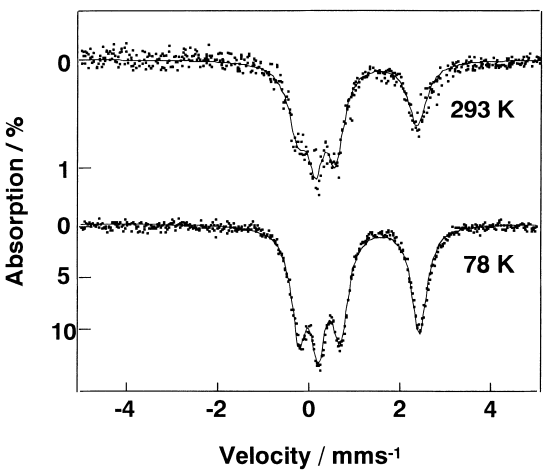

Fig. 6. Temperature dependence of the Mössbauer spectra of complex **2**.

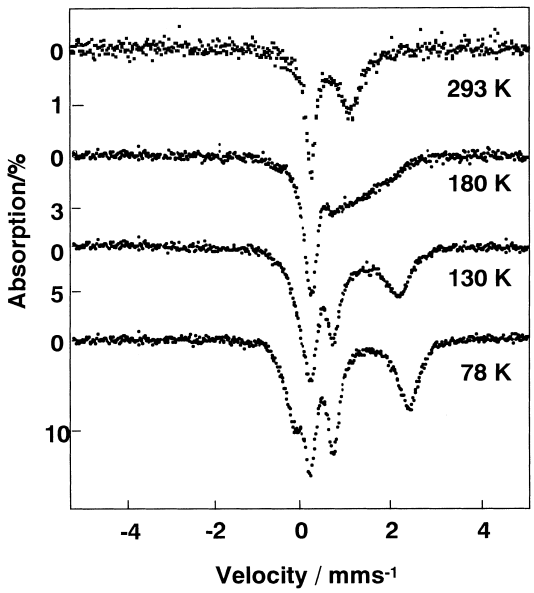

Fig. 7. Temperature dependence of the Mössbauer spectra of complex **3**.[13e)]

above three complexes is only the position of the methoxyl group in benzoic acid: 2- , 3- or 4-position. The difference results from the packing structure in the solid, rather than an electronic effect due to the displacement position of the methoxyl group, because it needs free space to experience a fast reorientation of iron moieties. 4-methoxybenzoic acid is more symmetric than 2- and 3-derivatives; symmetric bridging ligand leads to a symmetric packing of the complexes. It is assumed that the 3-derivative brings about a larger steric hindrance for reorientation than 2-derivatives. The temperature dependence of the Mössbauer spectra of **4** is complex, and thus difficult to understand. The Mössbauer spectra of **4** at variable temperature are shown in Fig. 8, and the Mössbauer parameters of the complexes are given in Table 5. The spectrum at 78 K is composed of iron(II) (δ = 1.01 mm/s, ΔE = 2.38 mm/s), iron(III) (δ = 0.42 mm/s, ΔE = 0.58 mm/s), and Fe^{ave} (δ = 0.74 mm/s, ΔE = 1.03 mm/s). The relative ratios of the absorption areas of iron(II), iron(III) and Fe^{ave} are 0.46, 0.42 and 0.12. The relative ratios of the absorption area of Fe^{ave} increase with rising temperature. As the temperature is increased, the two doublets of iron(II) and iron(III) gradually approach each other with line broadening to become a single average-valence doublet with δ of 0.65 mm s^{-1} and ΔE of 0.86 mm s^{-1}. These values are close to those of Fe^{ave}. It should be noted that a broadening of the lines of iron(II) and iron(III) is observed at 260 K, and that the FWHM of Fe^{ave} remains sharp. The isomer shifts of iron(II) and iron(III) approach each other and the isomers shift of Fe^{ave} is linearly decreased with rising in temperature, as shown in Fig. 9. These facts support that the spectra are a superposition of the relaxation spectra between iron(II) and iron(III), and of the spectrum of Fe^{ave}, and that the intramolecular electron transfer proceeds with accompanying phase transitions. The Mössbauer spectra of **5** are shown in Fig. 10. If the spectrum of **5** at 293 K is resolved with the two doublets composed of iron(II) and iron(III), the isomer shift of iron(II) is calculated to be 0.78 mm/s. The spectrum at 293 K

Table 5. Mössbauer Parameters of Complex **4**

T/K	δ/mm s^{-1}			ΔE_Q/mm s^{-1}			$\Gamma^{a)}$/mm s^{-1}			Area/%			$\Sigma\chi^2(\times 10^{-3})^{b)}$
	Fe^{2+}	Fe^{ave}	Fe^{3+}	Fe^{2+}	Fe^{ave}	Fe^{3+}	Fe^{2+}	Fe^{ave}	Fe^{3+}	Fe^{2+}	Fe^{ave}	Fe^{3+}	
78	1.01	0.74	0.42	2.38	1.03	0.58	0.87	0.30	0.65	46.27	11.69	42.04	5.81
200	0.76	0.73	0.45	1.85	1.02	0.62	0.50	0.52	0.68	31.92	32.32	35.76	0.69
220	0.72	0.72	0.46	1.72	1.01	0.66	0.50	0.38	0.74	28.90	39.21	31.89	0.82
240	0.70	0.69	0.47	1.59	1.00	0.68	0.57	0.43	0.61	29.35	41.50	29.15	0.55
260	0.67	0.66	0.48	1.50	0.93	0.70	0.57	0.42	0.43	29.90	44.22	25.88	0.83
293		0.65			0.86			0.28 0.51			100		0.67

a) Half width at half-maximum listed in order of increasing velocity of the peaks. b) Residual sum.

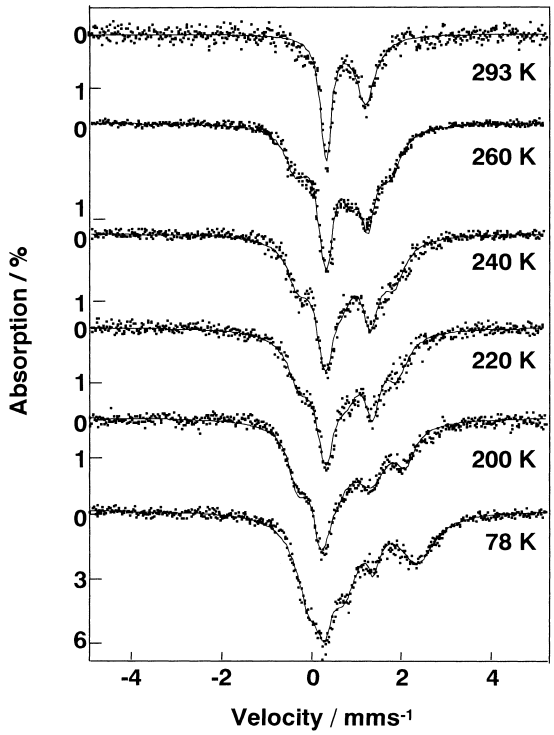

Fig. 8. Temperature dependence of the Mössbauer spectra of complex **4**.

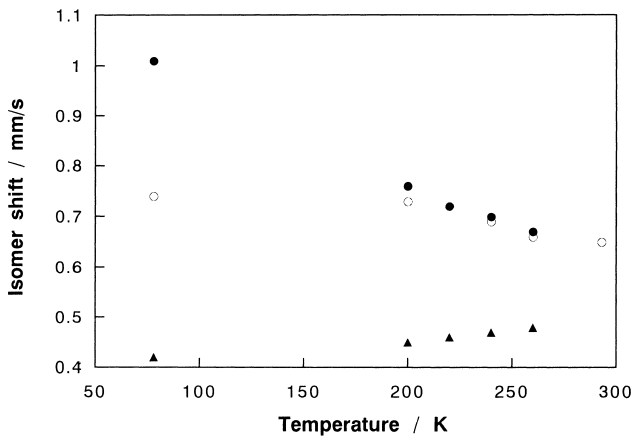

Fig. 9. Plots of the isomer shifts vs temperature of complex **4**; ● for iron(II); ▲ for iron(III); ○ for iron(ave.)

is similar to a relaxation spectrum with a correlation time $\tau =$

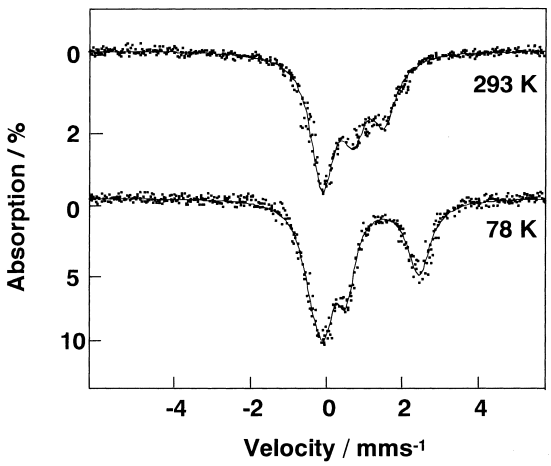

Fig. 10. Temperature dependence of the Mössbauer spectra of complex **5**.

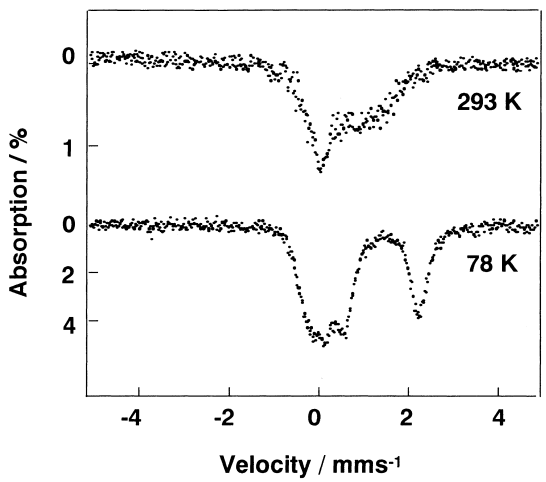

Fig. 11. Temperature dependence of the Mössbauer spectra of complex **6**.

5×10^{-7} s,[23] in which the theoretical spectra for the model was calculated using Wickman method.[24,13e] Complex **6** shows a localized Mössbauer spectrum at 78 K, as shown in Fig. 11. Two quadrupole doublets are seen at 78 K in the area ratio of nearly 1:1: Fe(II) with a δ of 1.13 mm s^{-1} and a ΔE of 2.46 mm s^{-1}, and Fe^{III} with a δ of 0.49 mm s^{-1} and a ΔE of 0.49 mm s^{-1}. The spectrum at 293 K shows the averaged valence states, and is similar to that of **1**.

A Grant-in-Aid for Scientific Research (No. 13440197) from the Ministry of Education, Science, Sports and Culture is greatly acknowledged.

References

1 a) R. E. Stenkamp, L. C. Sieker, L. H. Jensen, and J. Sanders-Loehr, *Nature* (*London*), **291**, 263 (1981). b) R. E. Stenkamp, L. C. Sieker, and L. H. Jensen, *J. Am. Chem. Soc.*, **106**, 618 (1984).

2 a) P. C. Wilkins and R. G. Wilkins, *Coord. Chem. Rev.*, **79**, 195 (1987). b) R. G. Wilkins and P. C. Harrington, *Adv. Inorg. Biochem.*, **5**, 51 (1983).

3 a) L. Yhelander and P. Reichard, *Annu. Rev. Biochem.*, **48**, 133(1979). b) P. Reichard and A. Ehrenberg, *Science*, **221**, 514(1987). c) B. M. Sjöberg, T. M. Loehr, and J. Sanders-Loehr, Jr., *J. Biochem.*, **21**, 96 (1982).

4 J. G. Dewitt, J. G. Bensten, A. C. Rosenzweig, B. Hedman, J. Green, S. Pilkington, G. C. Bensten, G. C. Papaefthymiou, H. Dalton, K. O. Hodgson, and S. J. Lippard, *J. Am. Chem. Soc.*, **113**, 9219 (1991).

5 B. G. Fox, W. A. Froland, J. E. Dege, and J. D. Lipsscomb, *J. Biol. Chem.*, **264**, 10023 (1989).

6 M. P. Woodland and H. Dalton, *J. Biol. Chem.*, **259**, 53 (1984).

7 a) B. A. Averill, J. G. Davis, S. Burman, T. Zirino, J. Sanders-Loehr, T. M. Loehr, J. T. Sage, and P. G. Debrunner, *J. Am. Chem. Soc.*, **109**, 3760 (1987). b) S. M. Kauzlarich, B. K. Teo, T. Zirino, S. Burman, J. C. Davis, and B. A. Averill, *Inorg. Chem.*, **25**, 2781 (1986).

8 E. Sinn, G. J. O'Connor, J. de Jersey, and B. Zerner, *Inorg. Chim. Acta*, **78**, L13 (1983).

9 M. Suzuki, A. Uehara, H. Oshio, K. Endo, M. Yanagi, S. Kida, and K. Saito, *Bull. Chem. Soc. Jpn.*, **60**, 3547 (1987).

10 M. Suzuki, A. Uehara, H. Oshio, K. Endo, M. Yanagi, S. Kida, and K. Saito, *Bull. Chem. Soc. Jpn.*, **61**, 3907 (1988).

11 a) A. S. Borovik, B. P. Murch, and L. Que, Jr., *J. Am. Chem. Soc.*, **109**, 7190 (1987). b) M. S. Mashuta, R. J. Webb, K. Oberhausen, J. F. Richardson, R. M. Buchanan, and D. N. Hendrickson, *J. Am. Chem. Soc.*, **111**, 2745 (1989). c) M. S. Mashuta, R. J. Webb, J. K. McCuske, E. A. Schmitt, K. J. Oberhausen, J. F. Richardson, R. M. Buchanan, and D. N. Hendrickson, *J. Am. Chem. Soc.*, **114**, 3815 (1992). d) A. S. Borovik, and L. Que, Jr., *J. Am. Chem. Soc.*, **110**, 2345(1988).

12 a) A. Neves, M. A. de Brito, I. Vencato, V. Drago, K. Griesar, and W. Haase, *Inorg. Chem.*, **35**, 2360(1996). b) C. Belle, I. Gautier-Luneau, J.-L. Pierre, and C. Scheer, *Inorg. Chem.*, **35**, 3706(1996).

13 a) Y. Maeda, Y. Tanigawa, S. Hayami, and Y. Takashima, *Chem. Lett.*, **1992**, 591 (1992). b) Y. Maeda, Y. Tanigawa, Y. Ando, Y. Takashima, and N. Matsumoto, *Acta Chim. Hung., Models in Chem.*, **130**, 55 (1993). c) Y. Maeda, Y. Tanigawa, N. Matsumoto, H. Oshio, M. Suzuki, and Y. Takashima, *Bull. Chem. Soc. Jpn.*, **67**, 125 (1994). d) Y. Maeda, K. Kawano, and T. Oniki, *J. Chem. Soc., Dalton Trans.*, **1995**, 3533(1995). e) T. Manago, S. Hayami, H. Oshio, S. Osaki, H. Hasuyama, R. H. Herber, and Y. Maeda, *J. Chem. Soc., Dalton Trans.*, **1999**, 1001 (1999).

14 G. Williams, G. R. Moore, and R. J. P. Williams, *Comments Inorg. Chem.*, **4**, 55 (1985).

15 N . S . Hush, M. N. Paddon-Row, E. Cotsaris, H. Oevering, J. W. Verhoeven, and M.Heppener, *Chem. Phys. Lett.*, **117**, 8 (1985).

16 T . Kambara and N. Sasaki, *J. Phys. Soc. Jpn.*, **51**, 1694 (1982).

17 a) S. H. Adachi, A. E. Panson, and R. M. Stratt, *J. Chem. Phys.*, **88**, 1134 (1988). b) D. N. Hendrickson, "Electron Transfer in Mixed-Valence Complexes in the Solid State," in "Mixed Valency Systems: Applications in Chemistry, Physics and Biology," NATO ASI Series C: Mathematical and Physical Sciences **343**, ed by K. Prassides, Kluwer Academic Publishers, Dordrecht, The Netherlands (1991), p 67–90. c) R. J. Webb, A. L. Rheingold, S. J. Geib, D. L. Staley, and D. N. Hendrickson, *Angew. Chem., Int. Ed. Engl.*, **28**, 1388 (1989). d) R. J. Webb, S. J. Geib, D. L. Staley, A. L. Rheingold, and D. N. Hendrickson, *J. Am. Chem. Soc.*, **112**, 5031 (1990). e) C.-C. Wu, H. G. Jang, A. L. Rheingold, P. Gütlich, and D. N. Hendrickson, *Inorg. Chem.*, **35**, 4137 (1996).

18 a) D. N. Hendrickson, S. M. Oh, T.-Y. Dong, T. Kambara, M. J. Cohn, and M. F. Moore, *Comments Inorg. Chem.*, **4**, 329 (1985). b) M. Sorai and D. N. Hendrickson, *Pure Appl. Chem.*, **63**, 1503 (1991).

19 a) H. Sano, *Hyperfine Interact.*, **53**, 97 (1990). b) S. Nakashima, A. Nishimori, Y. Masuda, H. Sano, and M. Sorai, *J. Phys. Chem. Solids*, **52**, 1169 (1991). c) K. Asamaki, T. Nakamoto, S. Kawata, H. Sano, M. Katada, and K. Endo, *Inorg. Chim. Acta*, **236**, 155 (1995).

20 L. O. Spreer, A. Li, D. B. MacQueen, C. B. Allan, J. W. Otvos, M. Calvin, R. B. Frankel, and G. C. Papaefthymiou, *Inorg. Chem.*, **33**, 1753(1994).

21 N. S. Hush, M. N. Paddon-Row, E. Cotsaris, H. Oevering, J. W. Verhoeven, and M. Heppener, *Chem. Phys. Lett.*, **117**, 8(1985).

22 M. B. Robin and P. Day, *Adv. Inorg. Chem. Radiochem.*, **10**, 247 (1967).

23 From the A. Ishida's paper for getting the master degree at Kyushu University. page 54, 2000.

24 H. H. Wickman, "Mössbauer Effect Methodology," ed by I. J. Gruverman, Plenum, New York (1966), pp.39–66.